SHAPE OPTIMIZATION OF SPATIAL CHEMOSTAT MODELS

MARIA CRESPO, BENJAMIN IVORRA,
ANGEL MANUEL RAMOS, ALAIN RAPAPORT

Communicated by Jesus Ildefonso Diaz

ABSTRACT. In this work, we study the shape optimization of a continuous bioreactor in which a substrate is degraded by a microbial ecosystem in a nonhomogeneous environment. The bioreactor considered here is a three-dimensional vertically oriented cylindrical tank. The behavior of reactants is described with a spatial chemostat model based on an Advection-Diffusion-Reaction system while the fluid flow is modeled using incompressible Navier-Stokes equations. We consider that the reaction rate between biomass and nutrient shows either monotonic or non-monotonic behavior. We tackle an optimization problem which aims to minimize the considered total reactor volume, with an output concentration (at stationary state) maintained below a desired threshold, by choosing a suitable bioreactor shape. We propose a methodology to create three different discrete parametrizations of the bioreactor geometry and obtain the optimized shapes with the help of a Hybrid Genetic Algorithm. We show that the optimized reactors exhibit height much larger than width and their exterior wall is concavely curved (the concavity at the upper part of the exterior wall being more pronounced for non-monotonic functions).

1. INTRODUCTION

Shape optimization has been extensively exploited in design engineering [3, 18, 30, 39, 33, 47, 48], particularly in aeronautical [6, 42, 44] and automotive areas [43, 68]. Traditionally, finding the optimal geometry of a particular device is based on a trial and error approach, in which, a number of prospective configurations is simulated and the results are compared. An alternative strategy relays in performing the mathematical modeling of the process, carrying out numerical simulations and solving the desired optimization problem with an appropriate optimization algorithm. Taking into consideration the exponential growth of the available computing power, this second approach provides a powerful computational tool able to simulate and analyze the efficiency of different geometry configurations.

In this work, we tackle the shape optimization of a continuous bioreactor. A bioreactor is a vessel in which microorganisms (e.g., bacteria), called biomass, are used to degrade a considered diluted substrate (e.g., nitrate). A reactor in which

substrate is continually added and product continually removed is called continuous bioreactor. The influence of the bioreactor design into the process efficiency has received considerable attention in the literature [21, 50, 57]. Most of the works are developed by experimentalists (see, e.g., [5, 7]) and focus on specific biological reactions occurring in continuous flow systems. Among the different reactor geometry configurations reviewed in literature, the most popular are flat-plate reactors [59, 64], torus-shaped reactors [49] and tubular reactors [56, 64]. In 2008, Xia et al. [67] showed that flow conditions (regarding mass transfer, shear stress, mixing, etc.) are strongly influenced by the reactor geometry, particularly at large scales. Nevertheless, computational fluid dynamics has not been commonly used to its full capacity to optimize reactor performance. Of particular interest are the works developed by Ansoni et al. [2] and Coenen et al. [8]. In [2], the authors consider a tubular reactor and model its hydrodynamics with 3D Navier-Stokes equations. They look for the optimal design (configuration of the inlet and the outlet pipes) of a given bioreactor, so that the dispersion of the residence time and the shear flow are minimized. These two concepts, related to fluid dynamics, are linked to the reactor effectiveness. In [8], the authors consider a cylindrical photobioreactor and model the dynamics of the organic compound with an advection-reaction equation. They look for the optimal geometry (radius and height) so that the reactant concentration at the outlet of the bioreactor is minimized.

We aim to solve the following design optimization problem: given the input reactant concentrations and the flow rate to be processed, what is the minimal reactor volume (and its shape) so that a desired output reactant concentration is attained? This problem has been modeled using ordinary differential equations (see, e.g., [17, 26, 28, 29, 41]) by approximating the behavior of a tubular device with a bioreactor composed by N well-mixed tanks in series. Then, the aim of the optimization becomes to find what are the volumes of the N tanks such that the total volume of the whole process is minimal. However, these studies suffer of two important drawbacks:

- While the proposed results are valid for small and medium sized systems, they do not describe the diffusion phenomena or the impact of fluid motions that may occur in larger tanks.
- The dimensioning parameters were not considered; only the total volume of the systems was optimized. However, in a real case, design parameters such as the diameter or the height of any biological or chemical system will influence its performance.

To overcome these drawbacks, we propose to couple hydrodynamics with biological phenomena occurring in a diffusive bioreactor. To do so, we use a particular spatial modeling based on Navier-Stokes equation (describing the fluid dynamics) together with an Advection-Diffusion-Reaction system (describing the behavior of the reactants in the bioreactor). We give a methodology to create three different discrete parametrizations of the bioreactor geometry and obtain the optimized shapes with the help of a Genetic Multi-layer Algorithm (GMA), a global optimization method based on the hybridization of a Multi-layer Secant method (MSA) [53, 54, 52], finding suitable initial conditions for a global optimization algorithm, with a given Genetic Algorithm (GA) [14, 23, 58, 66]. This kind of hybridization has been already tested for solving different optimization problems [24, 38] and, according to several numerical experiments, it seems that it achieves better results (in terms

of computational time and precision) than the GA used alone. The optimization problem is solved for monotonic and non-monotonic growth rate functions, in order to analyze the influence of the reaction into the optimal reactor configuration. In contrast to the previously cited experimental studies [5, 7, 56, 59], here, we do not specify beforehand a particular type of biological system but describe, in a general way, a biological substrate-biomass reaction in a continuous reactor. Compared to the works developed in [2, 8], we couple the fluid flow with the biological phenomena, while in[2, 8] the authors only model one of the two physics. Furthermore, in this case, the reactor geometry is parametrized with five variables (compared to the two-dimensional parametrization performed in [2, 8]) to be able to obtain a broader range of possible bioreactor shapes.

This article is organized as follows: Section 2 we introduce a mathematical model describing the dynamics of the bioreactor. In Section 3, we state the optimization problem which aims to minimize the considered reactor volume, with an outflow substrate concentration maintained to a desired threshold, by choosing a suitable bioreactor shape. In Section 4, we explain the numerical experiments carried out for the optimization problem and show the results. Section 5 draws the conclusions after the comparison between the obtained optimized reactors.

2. Mathematical Modeling

Let a vertical cylinder denoted by Ω^* be the domain of the bioreactor in consideration. When the problem is initialized, there is a certain amount of biomass inside Ω^* that reacts with the polluted water entering the device through the inlet Γ_{in}^* (the upper boundary of the cylinder). Treated water leaves the reactor through the outlet Γ_{out}^* (the lower boundary of the cylinder). We denote $\Gamma_{\text{wall}}^* = \delta\Omega^* \setminus (\Gamma_{\text{in}}^* \cup \Gamma_{\text{out}}^*)$, where null flux is considered.

We present the following model to describe the dynamics in the reactor, which includes advection-diffusion-reaction phenomena (see [10, 11, 12, 15]):

$$
\begin{aligned}
\frac{\mathrm{d}S}{\mathrm{d}t} &= \nabla \cdot (D_{\text{S}}\nabla S - \mathbf{u}S) - \mu(S)B \quad \text{in } \Omega^* \times (0, T), \\
\frac{\mathrm{d}B}{\mathrm{d}t} &= \nabla \cdot (D_{\text{B}}\nabla B - \mathbf{u}B) + \mu(S)B \quad \text{in } \in \Omega^* \times (0, T), \\
S(x, 0) &= S_0(x), \ B(x, 0) = B_0(x) \quad x \in \Omega^*, \\
\mathbf{n} \cdot (-D_{\text{S}}\nabla S + \mathbf{u}S) &= S_{\text{in}}u_3 \quad \text{in } \Gamma_{\text{in}}^* \times (0, T), \\
\mathbf{n} \cdot (-D_{\text{B}}\nabla B + \mathbf{u}B) &= 0 \quad \text{in } \Gamma_{\text{in}}^* \times (0, T), \\
\mathbf{n} \cdot (-D_{\text{S}}\nabla S) &= \mathbf{n} \cdot (-D_{\text{B}}\nabla B) = 0 \quad \text{in } \Gamma_{\text{out}}^* \times (0, T), \\
\mathbf{n} \cdot (-D_{\text{S}}\nabla S + \mathbf{u}S) &= \mathbf{n} \cdot (-D_{\text{B}}\nabla B + \mathbf{u}B) = 0 \quad \text{in } \Gamma_{\text{wall}}^* \times (0, T),
\end{aligned}
\tag{2.1}
$$

where $T > 0$ (s) is the length of the time interval for which we want to model the process, S (kg/m^3), B (kg/m^3) are the substrate and biomass concentrations inside the reactor which diffuse throughout the water in the vessel with diffusion coefficients D_{S} (m^2/s) and D_{B} (m^2/s), respectively, S_0 (kg/m^3), B_0 (kg/m^3) are the concentrations of substrate and biomass inside the bioreactor at the initial time, S_{in} (kg/m^3) is the substrate concentration that enters the reactor and $\mathbf{n}$ is the outward unit normal vector on the boundary of the domain Ω^*. Notice that besides the advection-diffusion terms, we also have a term corresponding to the reaction of biomass and substrate, governed by the growth rate function μ (s^{-1}).

We work with the following growth rate functions, which are extensively used in the literature – the Monod function [61, 27] is defined in $[0, +\infty)$ by

$$\mu(S) = \mu_{\max} \frac{S}{K_S + S}, \tag{2.2}$$

where $\mu_{\max}$ (s^{-1}) is the maximum specific growth rate and K_S (kg/m^3) is the half-saturation constant. The Haldane function [1, 27] is defined in $[0, +\infty)$ by

$$\mu(S) = \mu^* \frac{S}{K_S + S + S^2/K_I}, \tag{2.3}$$

where μ^* (s^{-1}) is the maximum specific growth rate in the absence of inhibition and K_I (kg/m^3) is the inhibition constant. Finally, vector $\mathbf{u} = (u_1, u_2, u_3)$ (m/s) is the flow velocity, which fulfills the following stationary Navier-Stokes equations for Newtonian incompressible viscous fluids (see, e.g., [22])

$$
\begin{aligned}
-\eta\Delta\mathbf{u} + \rho(\mathbf{u} \cdot \nabla)\mathbf{u} + \nabla p &= 0 \quad \text{in } \Omega^*, \\
\nabla \cdot \mathbf{u} &= 0 \quad \text{in } \Omega^*, \\
\mathbf{u} &= 0 \quad \text{in } \Gamma^*_{\text{wall}}, \\
\mathbf{u} &= -u_{\text{in}} \, E(x) \, \mathbf{n} \quad \forall x \in \Gamma^*_{\text{in}}, \\
\mathbf{n} \cdot (\eta\nabla\mathbf{u}) &= 0 \quad \text{in } \Gamma^*_{\text{out}}, \\
p(x) &= p_{\text{atm}} \quad \forall x \in \Gamma^*_{\text{out}},
\end{aligned}
\tag{2.4}
$$

where p is the pressure field (Pa); p_{atm} is the atmospheric pressure (Pa); η is the fluid dynamic viscosity (kg/m s); u_{in} (m/s) is the maximum injection velocity; E is the laminar flow inlet profile (a paraboloid of revolution) equal to 0 in the inlet border and unity in the inlet center; ρ is the fluid density (kg/ m^3), assumed constant through the reactor (as done, e.g., in [2, 8]).

Remark 2.1. Note that the flow field $\mathbf{u}$ has been considered stationary in order to reduce the computational complexity met when numerically solving system (2.1)-(2.4). This assumption is supported by numerical experiments, which seem to show that if we solve a time-dependent version of (2.4) coupled with (2.1), variable $\mathbf{u}$ approximates its stationary state much faster than variables (S, B).

Remark 2.2. According to [10], if $S_{\text{in}} \in L^\infty(0, T)$, $S_{\text{in}} \geq 0$ in $(0, T)$, $S_0 \in L^\infty(\Omega^*)$, $S_0 \geq 0$ in Ω^*, $B_0 \in L^\infty(\Omega^*)$ and $B_0 \geq 0$ in Ω^*, there exists a unique solution $(S, B) \in L^2(0, T; H^1(\Omega^*))^2 \cap \mathcal{C}(0, T, L^2(\Omega^*))^2 \cap L^\infty(\Omega^* \times (0, T))^2$ of system (2.1)-(2.4).

As we will see in Section 4, we aim to find stationary solutions of system (2.1), which we denote by $(\hat{S}, \hat{B})$. A usual way to get them is to solve numerically (2.1) and then consider its solution for a time value $\hat{T}$ (large enough) as the steady-state solution. This is usually computationally easier (see, e.g., [40]) and allows us to recover non-trivial stationary solutions (different to $(\hat{S}, \hat{B}) = (S_{\text{in}}, 0)$) by choosing appropriate initial conditions.

3. Optimization problem

Here, we optimize the main design parameters (reactor shape and total volume) with respect to the output concentration. More precisely, in Section (3.1) we introduce the general formulation of the considered continuous optimization problem.

Then, in Section (3.2) we propose three particular discrete implementations of this problem to be solved numerically in Section 4.

3.1. **General problem.** Let us consider cylindrical bioreactors Ω^* which are empty solids of revolution, and so, they can be described by using a 2D domain $\Omega \subset \mathbb{R}^2$ (similar to the one depicted by Figure 1) by using cylindrical coordinates (r, z), where r is the distance to the cylinder axis. The simplified domain Ω is described as follows: H (m) is the bioreactor height; r (m) is the radius of the inlet Γ_{in} and the outlet Γ_{out}; h (m) is the height of the inlet and outlet pipes; R_1 (m) and R_2 (m) are the radius of the bioreactor wall perpendicular to the inlet and outlet pipes, respectively; the curve of the exterior wall corresponds to the graph of the function $\psi : [h, H - h] \to [r, +\infty)$, which satisfies $\psi(h) = R_2$ and $\psi(H - h) = R_1$. Since, in practice, the inlet and outlet pipes have standard dimensions (depending on the desired industrial application), we assume that r and h have fixed values. Similarly, we take into account that the height and width of the reactor cannot exceed certain values (for example, due to a limitation of the physical space in an industrial factory).
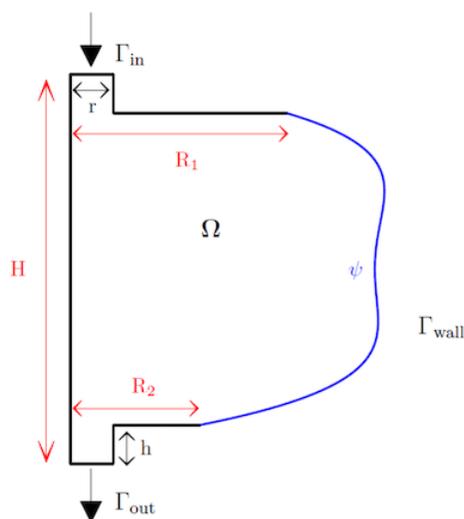

FIGURE 1. Schematic representation of the bioreactor geometries used to solve problem (3.1). The exterior curve (depicted in blue), which corresponds to part of the bioreactor exterior wall, is defined as $(z, \psi(z))$, where $z \in [h, H - h]$.

Given a prescribed output substrate concentration S_{lim} (kg/m^3), we state the following optimization problem

$$\text{Find } \phi^{\text{opt}} \in \Phi, \text{ such that}$$

$$\text{Vol}(\phi^{\text{opt}}) = \min_{\phi \in \Phi} \text{Vol}(\phi), \tag{3.1}$$

$$\hat{S}_{\text{out}}(\phi^{\text{opt}}) \leq S_{\text{lim}},$$

where $\phi = (H, R_1, R_2, \psi) \in \Phi$ defines a particular bioreactor shape and $\Phi = \{[H_{\min}, H_{\max}] \times [r, R_{1,\max}] \times [r, R_{2,\max}] \times \mathcal{C}([h, H - h], [r, R_{\max}])\}$ is the admissible

space; $\mathrm{Vol}(\phi)$ (m^3) is the volume of the reactor, computed as

$$\mathrm{Vol}(\phi) = \int_{\Omega^*(\phi)} \mathrm{d}x\mathrm{d}y\mathrm{d}z, \tag{3.2}$$

with $\Omega \subset \mathbb{R}^2$ being the (r,z)-domain obtained with the set ϕ and $\Omega^*(\phi) \subset \mathbb{R}^3$ is the corresponding 3D domain; and $\hat{S}_{\mathrm{out}}(\phi)$ (kg/m^3) denotes an average of the concentration of substrate that leaves the bioreactor (at steady state), computed as

$$\hat{S}_{\mathrm{out}}(\phi) = \frac{\int_{\Gamma_{\mathrm{out}}^*} S_\phi(x,y,0,\hat{T})|u_3(x,y,0)|\mathrm{d}x\mathrm{d}y}{\int_{\Gamma_{\mathrm{out}}^*} |u_3(x,y,0)|\mathrm{d}x\mathrm{d}y}, \tag{3.3}$$

with $S_\phi(\cdot,\cdot,\cdot,\hat{T})$ the solution of system (2.1), obtained with the 3D domain $\Omega^*(\phi)$, at time $\hat{T}$ and u_3 the third component of the velocity vector in (2.4).

Remark 3.1. In practice, we aim to improve (in terms of reactor volume) a given bioreactor which attains the prescribed output substrate concentration and we choose the admissible space Φ so that it accounts for the geometry of the given vessel. Therefore, if problem (3.1) does not have a solution is because the minimum does not exist (only an infimum value is ensured). For the numerical experiments considered in Section 4, we look for one of the optimal solutions of the discretized problems (3.5), (3.6) and (3.9), whose existence is guaranteed because of the compactness of the selected admissible spaces $\tilde{\Phi}^i$ ($i = 1,2,3$).

3.2. **Numerical problem.** Here, we present three discrete versions of the optimization problem (3.1), related to three different discrete parametrizations of the bioreactor geometry. The parametrization proposed in Section 3.2.1 allows us to model tubular shapes (typically used in the industry sector), while the parametrizations in Sections 3.2.2 and 3.2.1 offer the possibility to obtain a wider range of reactor geometries. We solve the discrete optimization problems (3.5), (3.6) and (3.9) by using the Hybrid Genetic Algorithm, and its parameters, presented in Section 3.2.4.

For the sake of simplicity, the objective function and the restriction in problem (3.1) are combined into a new objective function $J(\phi)$ (m^3) as

$$J(\phi) = \mathrm{Vol}(\phi)\Big(1 + \beta \frac{\max(\hat{S}_{\mathrm{out}}(\phi) - S_{\mathrm{lim}}, 0)}{S_{\mathrm{lim}}}\Big), \tag{3.4}$$

where β is a free parameter (usually large) and the term multiplied by the coefficient β is a barrier function used to penalize solutions with S_{lim} smaller than an average of the substrate concentration exiting the bioreactor. Introducing the penalty term in (3.4) allows us to solve problem (3.1) with the unconstrained (low-cost) optimization algorithm proposed in Section 3.2.4. This approach has been previously used in the literature for solving computationally expensive industrial optimization problems (see, e.g. [35]). As it is typically done when performing optimization with a penalty method, the value of the penalty parameter β is usually obtained by performing several tests (see [45, Chapter 15.1]).

3.2.1. *Parametrization 1.* As a first approach, we consider bioreactor geometries as depicted in Figure 2-(a). The exterior wall corresponds to the segment $[h, H -$
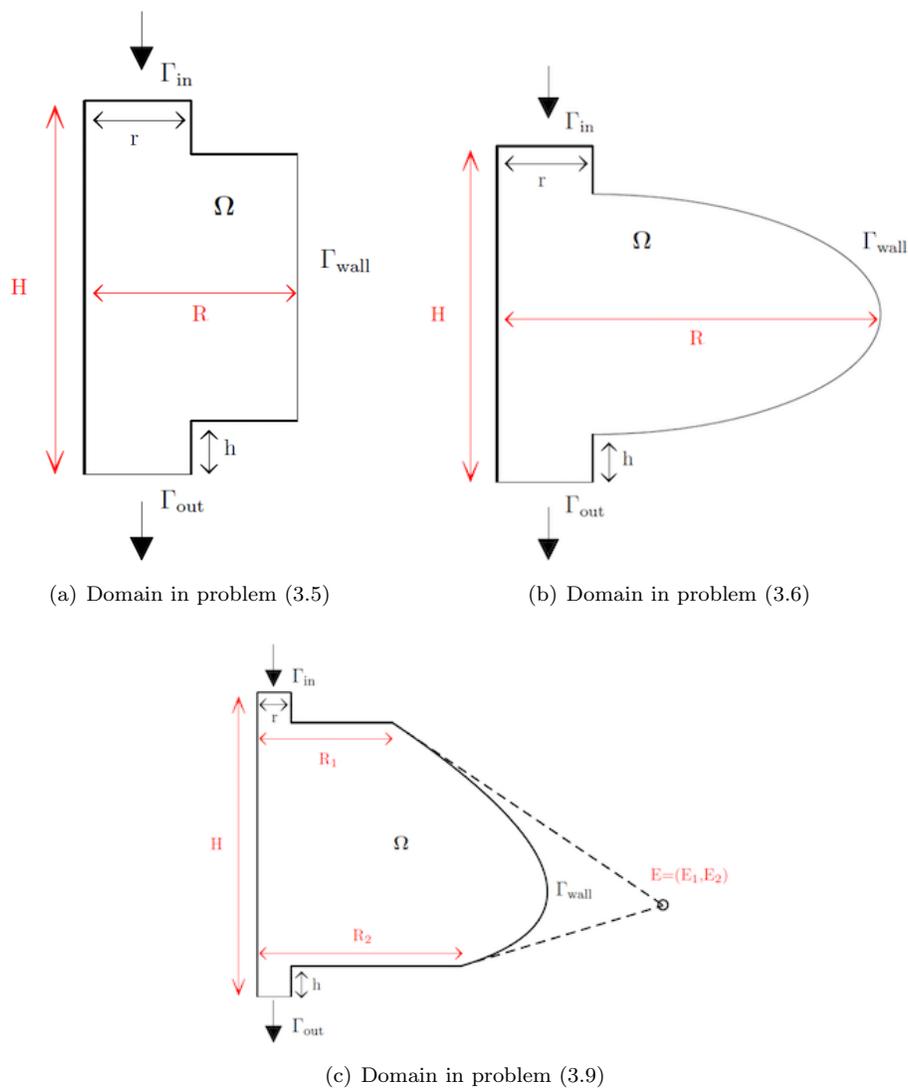
(a) Domain in problem (3.5)

(b) Domain in problem (3.6)

(c) Domain in problem (3.9)

FIGURE 2. Schematic representation of the bioreactor geometries used to solve the discrete problems (3.5), (3.6) and (3.9).

$h] \times \{R\}$, where $R \in [r, R_{\max}]$ (m). The variable ϕ in problem (3.1) is taken as $\phi = (H, R, R, \psi)$, where $\psi : [h, H - h] \to [r, R_{\max}]$ with

$$\psi(z) = R.$$

In this case, the bioreactor geometry only depends on parameters H and R and the optimization problem (3.1) can be reformulated as

Find $\tilde{\phi}^{1,\mathrm{opt}} \in \tilde{\Phi}^1$, such that

$$J(\tilde{\phi}^{1,\mathrm{opt}}) = \min_{\tilde{\phi}^1 \in \tilde{\Phi}^1} J(\tilde{\phi}^1), \tag{3.5}$$

where $\tilde{\phi}^{1,\mathrm{opt}} = (H^{\mathrm{opt}}, R^{\mathrm{opt}})$ and $\tilde{\Phi}^1 := \{(H, R) \in [H_{\min}, H_{\max}] \times [r, R_{\max}]\} \subset \mathbb{R}^2$ is the admissible space.

3.2.2. *Parametrization 2.*

As a second approach, we consider bioreactor geometries as depicted in Figure 2-(b). The exterior wall corresponds to a semi-ellipse with center $(r, \frac{H}{2})$ and with lengths of the semi-axis given by the pair $(R - r, \frac{H-2h}{2})$, where $R \in [r, R_{\max}]$ (m). The variable ϕ in problem (3.1) is taken as $\phi = (H, r, r, \psi)$, where $\psi : [h, H - h] \to [r, R_{\max}]$ with

$$\psi(z) = r + (R - r)\sqrt{1 - \left(\frac{z - H/2}{h - H/2}\right)^2}.$$

It is straightforward to see that, if $R \in [r, R_{\max}]$, then $\psi \in \mathcal{C}([h, H - h], [r, R_{\max}])$.

As in problem (3.5), the bioreactor geometry only depends on parameters H and R and the optimization problem (3.1) can be reformulated as

$$\text{Find } \tilde{\phi}^{2,\mathrm{opt}} \in \tilde{\Phi}^2, \text{ such that}$$
$$J(\tilde{\phi}^{2,\mathrm{opt}}) = \min_{\tilde{\phi}^2 \in \tilde{\Phi}^2} J(\tilde{\phi}^2), \tag{3.6}$$

where $\tilde{\phi}^{2,\mathrm{opt}} = (H^{\mathrm{opt}}, R^{\mathrm{opt}})$ and $\tilde{\Phi}^2 := \{(H, R) \in [H_{\min}, H_{\max}] \times [r, R_{\max}]\} \subset \mathbb{R}^2$ is the admissible space.

3.2.3. *Parametrization 3.*

As a third approach, we consider bioreactor geometries as depicted in Figure 2-(c). The shape of the exterior wall is a quadratic *Bézier curve* (see, for example, [19]), associated with the control points $\mathbf{P} = (R_1, H - h)$, $\mathbf{Q} = (R_2, h)$ and $\mathbf{E} = (E_1, E_2)$, where $(E_1, E_2) \in [E_{1,\min}, E_{1,\max}] \times [E_{2,\min}, E_{2,\max}])$, by the formula

$$\mathbf{B}(\sigma) = (B_1(\sigma), B_2(\sigma)) = (1 - \sigma)^2 \mathbf{P} + 2(1 - \sigma)\sigma \mathbf{E} + \sigma^2 \mathbf{Q}, \quad \sigma \in [0, 1]. \tag{3.7}$$

The variable ϕ appearing in problem (3.1) is taken as $\phi = (H, R_1, R_2, \psi)$, where $\psi : [h, H - h] \to [r, R_{\max}]$ wiht

$$\psi(z) = B_1(B_2^{-1}(z)).$$

To assure that $\psi([h, H - h]) \subseteq [r, R_{\max}]$, we impose the radius expansions R_1 and R_2 to lie in the segment $[r, R_{\max}]$. Once R_1 and R_2 have been chosen we take $E_{1,\min}$ and $E_{1,\max}$ as in Lemma 3.2 below so that $B_1 \circ B_2^{-1} \in \mathcal{C}([h, H - h], [r, R_{\max}])$. Furthermore, we take $E_{2,\min} = h$ and $E_{2,\max} = H - h$.

Now, we define two new optimization parameters $\alpha_1, \alpha_2 \in [0, 1]$ such that

$$E_1 = E_{1,\min} + \alpha_1 \cdot (E_{1,\max} - E_{1,\min}) \quad \text{and} \quad E_2 = h + \alpha_2 \cdot (H - 2h). \tag{3.8}$$

In that case, the bioreactor geometry only depends on parameters H, R_1, R_2, α_1 and α_2. The solution of the optimization problem (3.1) is approximated by computing

$$\text{Find } \tilde{\phi}^{3,\mathrm{opt}} \in \tilde{\Phi}^3, \text{ such that}$$
$$J(\tilde{\phi}^{3,\mathrm{opt}}) = \min_{\tilde{\phi}^3 \in \tilde{\Phi}^3} J(\tilde{\phi}^3), \tag{3.9}$$

where $\tilde{\phi}^{3,\mathrm{opt}} = (H^{\mathrm{opt}}, R_1^{\mathrm{opt}}, R_2^{\mathrm{opt}}, \alpha_1^{\mathrm{opt}}, \alpha_2^{\mathrm{opt}})$ and

$$\tilde{\Phi}^3 := \{(H, R_1, R_2, \alpha_1, \alpha_2) \in [H_{\min}, H_{\max}] \times [r, R_{1,\max}] \times [r, R_{2,\max}] \times [0, 1]^2\} \subset \mathbb{R}^5$$

is the admissible space, with $R_{i,\max} \leq R_{\max}$ for $i = 1, 2$.

Lemma 3.2. *Let us denote $E_{1,\min} = r - \sqrt{(R_1 - r)(R_2 - r)}$ and $E_{1,\max} = R_{\max} + \sqrt{(R_1 - R_{\max})(R_2 - R_{\max})}$. If $(E_1, E_2) \in [E_{1,\min}, E_{1,\max}] \times [h, H - h]$, then $B_1 \circ B_2^{-1} \in \mathcal{C}([h, H - h], [r, R_{\max}])$.*

Proof. We divide the proof in four steps:

Step 1. Let us prove that, if $E_2 \in [h, H - h]$, then $B_2([0,1]) = [h, H - h]$. To obtain the minimum and maximum values of $B_2(\sigma)$, $\sigma \in [0,1]$, we compute the critical points σ_2^* satisfying the equation $\frac{\mathrm{d}B_2}{\mathrm{d}\sigma}(\sigma_2^*) = 0$ on the interior of $]0,1[$. When considering E_2 as a variable, one can see that σ_2^* depends on E_2 through the expression $\sigma_2^*(E_2) = \frac{E_2 - H + h}{2E_2 - H}$, with corresponding value $B_2(\sigma_2^*(E_2)) = \frac{E_2^2 + h^2 - Hh}{2E_2 - h}$. Now, to find the lower and upper bounds for variable E_2 (assuring that $B_2(\sigma) \in [h, H - h] \ \forall \sigma \in [0,1]$), we respectively solve equations $B_2(\sigma_2^*(E_{2,\mathrm{m}})) = h$ and $B_2(\sigma_2^*(E_{2,\mathrm{M}})) = H - h$. It is easy to prove that the unique solutions of these equations are $E_{2,\mathrm{m}} = h$ and $E_{2,\mathrm{M}} = H - h$. Finally, taking into account that $\frac{\mathrm{d}B_2^2}{\mathrm{d}\sigma^2} = 2H - 4E_2$, it follows that $\frac{\mathrm{d}^2 B_2}{\mathrm{d}\sigma^2}\big|_{E_2 = h} = 2(H - 2h) > 0$ and $\frac{\mathrm{d}^2 B_2}{\mathrm{d}\sigma^2}\big|_{E_2 = H - h} = 2(2h - H) < 0$, and so, one can conclude that $E_{2,\min} = h$ and $E_{2,\max} = H - h$.

Step 2. Let us prove that the function $B_2 : [0,1] \to [h, H - h]$ is injective. Let $\sigma, \bar{\sigma} \in [0,1]$ satisfying $B_2(\sigma) = B_2(\bar{\sigma})$. By definition, this implies that

$$(1 - \sigma)^2 (H - h) + 2(1 - \sigma)\sigma E_2 + \sigma^2 h = (1 - \bar{\sigma})^2 (H - h) + 2(1 - \bar{\sigma})\bar{\sigma} E_2 + \bar{\sigma}^2 h.$$

Easy calculations lead to

$$(H - h)\big(\sigma^2 - \bar{\sigma}^2 - 2\sigma + 2\bar{\sigma}\big) + 2E_2\big(\sigma - \bar{\sigma} - \sigma^2 + \bar{\sigma}^2\big) + h\big(\sigma^2 - \bar{\sigma}^2\big) = 0.$$

Denoting $x = \bar{\sigma} - \sigma$ and $y = \bar{\sigma} + \sigma$, the previous equation can be rewritten as

$$x(2 - y)(H - h) + 2x(y - 1)E_2 - xyh = 0$$
$$\Leftrightarrow x\left(2(H - h) - 2E_2 + y(2E_2 - H)\right) = 0.$$

This implies that either $x = 0$ or $y = \frac{2(H - h - E_2)}{H - 2E_2}$. In the second case, it is easy to see that $y = 1 + \frac{H - 2h}{H - 2E_2}$ and, since we assume that $E_2 > h$, it follows that $y > 2$, but this enters in a contradiction with the definition of y. Thus, we can conclude that $x = 0$, so $\sigma = \bar{\sigma}$ and the injectivity is proved.

Step 3. Let us prove that, if $E_1 \in [E_{1,\min}, E_{1,\max}]$, then $B_1([0,1]) = [r, R_{\max}]$.

Similarly to step 1, to obtain the minimum and maximum values of $B_1(\sigma)$, $\sigma \in [0,1]$, we compute the critical points σ_1^* satisfying the equation $\frac{\mathrm{d}B_1}{\mathrm{d}\sigma}(\sigma_1^*) = 0$ on the interior of the domain. When considering E_1 as a variable, one can see that σ_1^* depends on E_1 through the expression $\sigma_1^*(E_1) = \frac{R_1 - E_1}{R_1 + R_2 - 2E_1}$, with corresponding value $B_1(\sigma_1^*(E_1)) = \frac{R_1 R_2 - E_1^2}{R_1 + R_2 - 2E_1}$. Now, to obtain lower and upper bounds for the variable E_1 (assuring that $B_1(\sigma) \in [r, R_{\max}] \ \forall \sigma \in [0,1]$), we respectively solve equations $B_1(\sigma_1^*(E_{1,\mathrm{m}})) = r$ and $B_1(\sigma_1^*(E_{1,\mathrm{M}})) = R_{\max}$. Each of these equations has two solutions, given by $E_{1,\mathrm{m}}^{\pm} = r \pm \sqrt{(R_1 - r)(R_2 - r)}$ and $E_{1,\mathrm{M}}^{\pm} = R_{\max} \pm \sqrt{(R_1 - R_{\max})(R_2 - R_{\max})}$. Taking into account that $\frac{\mathrm{d}^2 B_1}{\mathrm{d}\sigma^2} = 2(R_1 + R_2 - 2E_1)$,

$$\frac{\mathrm{d}^2 B_1}{\mathrm{d}\sigma^2}\big|_{E_1 = E_{1,\mathrm{m}}^{\pm}} = 2(R_1 + R_2 - 2r) \mp 4\sqrt{(R_1 - r)(R_2 - r)}$$

and

$$\frac{\mathrm{d}^2 B_1}{\mathrm{d}\sigma^2}\big|_{E_1 = E_{1,\mathrm{M}}^{\pm}} = 2(R_1 + R_2 - 2R_{\max}) \mp 4\sqrt{(R_1 - R_{\max})(R_2 - R_{\max})},$$

and so, one can conclude that $E_{1,\min} = E_{1,m}^-$ and $E_{1,\max} = E_{1,M}^+$.

Step 4. Let us prove that $B_1 \circ B_2^{-1} \in \mathcal{C}([h, H-h], [r, R_{\max}])$. Since $B_1 : [0,1] \to [r, R_{\max}]$ and $B_2 : [0,1] \to [h, H-h]$ are continuous functions and B_2 is injective, we conclude that $B_1 \circ B_2^{-1}$ is well defined and continuous because it is the composition of continuous functions. $\qquad\square$

3.2.4. *Optimization algorithm.* In this section, we describe in detail the optimization algorithm and the parameters used to solve numerical problems (3.5), (3.6) and (3.9). For the sake of simplicity, here, we consider a general optimization problem

$$\min_{x \in \Theta} J(x) \tag{3.10}$$

where $J : x \to \mathbb{R}$ is the fitness function; x is the optimization parameter, $\Theta \subset \mathbb{R}^N$, with $N \in \mathbb{N}$, is the search space. Notice that in order to recover problems (3.5), (3.6) and (3.9) one should replace $x = \tilde{\phi}^i$ ($i = 1,2,3$), $\Theta = \tilde{\Phi}^i$ ($i = 1,2,3$) and $N = 2, 2, 5$ in the general problem formulation (3.10).

The proposed algorithm, called Genetic Multi-Layer Algorithm (GMA), is a global optimization method based on a hybridization between a genetic algorithm (GA) [14, 23, 58, 66] (which performs a global search of the solution) and a multilayer secant method (MSA) [53, 54, 52] (which provides suitable initial populations for the GA). A complete validation of these algorithms on various industrial problems can be found in [24, 30, 37, 34, 38, 35, 39, 36, 31] and references therein. Broadly speaking, GAs are search techniques which try to solve problems similar to (3.10) through a stochastic process based on a natural selection process that mimics biological evolution. The GAs have many advantages as, for example, they can solve complex optimization problems (e.g., with high dimensional search space or function with various with local minima). However, they exhibit lower accuracy than other methods, such as gradient algorithms. Before explaining the methodology used to enhance these inconveniences, we detail the GA used in this work.

Genetic algorithm scheme:

Step 1. Inputs: The user must define six parameters: $N_p \in \mathbb{N}$, $N_g \in \mathbb{N}$, $p_c \in [0,1]$, $p_m \in [0,1]$, $\lambda \in \mathbb{R}$ and $\hat{g} \in \mathbb{N}$, the meaning of which is clarified later in the following steps. In addition, the user needs to provide a first set, called *initial population* and denoted by $X^0 = \{x_j^0 \in \Phi, j = 1, \ldots, N_p\} \in \Theta$, *of* N_p possible solutions of the optimization problem (3.10). Each row x_j^0 in X^0 ($j = 1, \ldots, N_p$) is called *individual*, while each component $x_{j,k}^0$ of an individual ($k = 1, \ldots, N$) is called *gene*. In our case $\Theta = \prod_{k=1}^N [l_k, u_k]$, where l_k and u_k are respectively the lower and upper bounds *of* the gene $x_{j,k}^i$.

Step 2. Generation of new populations: Starting from the initial population X^0, we recursively create $N_g \in \mathbb{N}$ new populations, which we call *generations*, by applying 4 stochastic steps, called *selection*, *crossover*, *mutation* and *elitism*, which are described in Steps 3.1, 3.2, 3.3 and 3.4, respectively. More precisely, let $X^i = \{x_j^i \in \Theta, j = 1, dots, N_p\}$ with $i = 1, \ldots, N_g - 1$, denotes the population at iteration i. Thus, using the following (N_p, N)-real valued matrix notation

$$X^i = \begin{bmatrix} x_1^i(1) & \cdots & x_1^i(N) \\ \vdots & \vdots & \vdots \\ x_{N_p}^i(1) & \cdots & x_{N_p}^i(N) \end{bmatrix},$$

X^{i+1} is obtained by considering

$$X^{i+1} = (I_N - \mathcal{E}^i)(\mathcal{C}^i \mathcal{S}^i X^i + \mathcal{M}^i) + \mathcal{E}^i X^i \qquad (3.11)$$

where matrices $\mathcal{S}^i$, $\mathcal{C}^i$, $\mathcal{M}^i$, $\mathcal{E}^i$ and I_N are described below.

Step 2.1 Selection: This operator is used to select individuals according to their fitness value. There exist various selection techniques (see, for instance, [23, 58, 66]), among which we use the *Roulette Wheel Selection* method. We randomly select N_p individuals from X^i with eventual repetitions. Each individual $x_j^i \in X^i$, with $j = 1, \dots, N_p$ has a probability to be selected during this process which is given by $J(x_j^i)^{-1} / \sum_{k=1}^{N_p} J(x_k^i)^{-1}$. This step can be summarized as

$$X^{i+1,1} = \mathcal{S}^i X^i,$$

where $\mathcal{S}^i$ is a binary valued (N_p, N_p)-matrix satisfying $S_{j,k}^i = 1$ if the k-th individual in X^i is the j-th selected individual, and $S_{j,k}^i = 0$ in other case.

Step 2.2 Crossover: This operator is used to create a new individual by combining the genes of two existing individuals from the population X^i (chosen during the previous selection process). There are several methods for combining individuals (see, for instance, [14, 23, 58]), among which we use the *Arithmetic Crossover* method. For each pair of consecutive individuals (rows) $2j - 1$ and $2j$ in $X^{i+1,1}$, with $1 \le j \le \text{floor}(N_p/2)$ (where $\text{floor}(a)$ is the nearest integer lower than or equal to a), we determine, with a probability p_c, if those rows exchange data or if they are directly copied into an intermediate population denoted by $X^{i+1,2}$. Thus, matrix $\mathcal{C}^i$ is a real valued matrix of size (N_p, N_p), satisfying

$$\mathcal{C}_{2j-1,2j-1}^i = \lambda_1, \quad \mathcal{C}_{2j-1,2j}^i = 1 - \lambda_1, \quad \mathcal{C}_{2j,2j}^i = \lambda_2, \quad \mathcal{C}_{2j,2j-1}^i = 1 - \lambda_2,$$

where $\lambda_1 = \lambda_2 = 1$ with probability $1 - p_c$, or λ_1, λ_2 are randomly chosen in $(0, 1)$ considering a uniform distribution, in other case. Other coefficients of $\mathcal{C}^i$ are set to 0. If N_p is odd, then we also set $\mathcal{C}^i(N_p, N_p) = 1$, and then the N_p-th row of $X^{i+1,1}$ is directly copied into $X^{i+1,2}$.

Step 2.3 Mutation: This operator randomly modifies the value of one or more genes of an individual from the population $X^{i+1,2}$ (obtained during the previous crossover process). It provides diversity in the population and intends to avoid the premature convergence phenomenon (i.e., population concentrated near a local minimum, see [23]). Each individual can be mutated with a probability p_m given by the user. There exist different techniques to randomly mutate individuals (see, for instance, [14, 58]), among which we use the *Non-Uniform Mutation* method. We decide, with a probability p_m, if each row of $X^{i+1,2}$ is randomly perturbed or not. This step is defined by

$$X^{i+1,3} = X^{i+1,2} + \mathcal{M}^i,$$

where $\mathcal{M}^i$ is a real valued matrix with size (N_p, N) and the j-th row satisfies

$$\mathcal{M}_j^i = \begin{cases} \vec{0} & \text{with probability } 1 - p_m \\ \Delta(g, x_j^i) & \text{in other case} \end{cases}$$

and the k-th component of the vector $\Delta(g, x_j^i)$ is defined as

$$\Delta(g, x_j^i) = \begin{cases} (u_k - x_{j,k}^i)(1 - \gamma^{(1 - \frac{g}{N_g})^\lambda}) & \text{if } \tau = 0 \\ (l_k - x_{j,k}^i)(1 - \gamma^{(1 - \frac{g}{N_g})^\lambda}) & \text{if } \tau = 1 \end{cases}$$

where g is the current generation number, τ is a binary random number, γ is a uniform random number in $[0, 1]$ and λ is a parameter given by the user, determining the degree of dependency on the iteration number. This mutation method decreases the mutation rate as the generation number increases.

Step 2.4 Elitism: This operator ensures that at least one of the best individuals of the current generation is directly copied to the next generation. The main advantage of elitism is that a decreasing convergence is guaranteed. For more details about elitism methods see, for instance, [58, 66].

Let x_b^i, where $b \in 1, \ldots, N_{\mathrm{p}}$, be the individual in X^i with the lowest value of the fitness function (or, if there exist various, one of those individuals selected randomly with a uniform distribution). If x_b^i has a lower fitness value than all the individuals in $X^{i+1,3}$, it is directly copied at the b-th row of X^{i+1}. This step can be formalized as

$$X^{i+1} = (I_N - \mathcal{E}^i)(X^{i+1,3}) + \mathcal{E}^i X^i,$$

where I_N is the identity matrix of size N and $\mathcal{E}^i$ is a real-valued $(N_{\mathrm{p}}, N_{\mathrm{p}})$-matrix such that $\mathcal{E}^i(b, b) = 1$ if x_b^i has a lower fitness value than all the individuals in $X^{i+1,3}$ and 0 otherwise, $\mathcal{E}^i = 0$ elsewhere.

The genetic search is terminated when N_{g} generations have been computed, or after a number of generations specified by the user, $\hat{g}$, without improvement of the fitness value (i.e., the fitness of the best element has not decreased).

Step 3. Output: When GA stops, it returns, as an output solution, the individual who has the lowest value for the objective function J among all the individuals in all the populations considered during the whole evolving process, i.e.,

$$GAO(X^0; N_{\mathrm{p}}; N_{\mathrm{g}} : p_{\mathrm{m}}; p_{\mathrm{c}}; \lambda; \hat{g})$$
$$= \mathrm{argmin}\left\{ J(x_i^j) \mid x_i^j \text{ is the -th row of } X^i, \ i = 1, \ldots, N_{\mathrm{g}}, \ j = 1, \ldots, N_{\mathrm{p}} \right\}.$$

As said at the beginning of this section, to accelerate the convergence and improve the accuracy of the above-described GA, we combine it with the MSA described below to build a hybrid algorithm, called GMA. Its general scheme is as follows:

Genetic multi-Layer algorithm scheme:

Step 1. Inputs: The user must define seven parameters: $s_{\max} \in \mathbb{N}$, $N_{\mathrm{p}} \in \mathbb{N}$, $N_{\mathrm{g}} \in \mathbb{N}$, $p_{\mathrm{c}} \in [0, 1]$, $p_{\mathrm{m}} \in [0, 1]$, $\lambda \in \mathbb{R}$ and $\hat{g} \in \mathbb{N}$. $s_{\max}$ denotes the number of iterations of the MSA.

Step 2. Initial population: A first family of possible solutions of the optimization problem (3.10), denoted by $X_1^0 = \{x_{1,j}^0 \in \Theta, j = 1, \ldots, N_{\mathrm{p}}\}$, is randomly generated in the search space Θ considering a uniform distribution.

Step 3. Main loop: For s from 1 to $s_{\max}$:

Step 3.1 We run the GA starting from the initial population X_s^0 and obtain the optimal individual $o_s = GAO(X_s^0, N_{\mathrm{p}}, N_{\mathrm{g}}, p_{\mathrm{m}}, p_{\mathrm{c}}, \lambda, \hat{g})$.

Step 3.2 We build a new initial population for the GA, $X_{s+1}^0 = \{x_{s+1,j}^0 \in \Theta, j = 1, \ldots, N_{\mathrm{p}}\}$, by considering a secant method between each element in X_s^0 and the optimal individual o_s, i.e., for all $j \in \{1, \ldots, N_{\mathrm{p}}\}$, if $J(o_s) = J(x_{s,j}^0)$ we set

$$x_{s+1,j}^0 = x_{s,j}^0,$$

else we set

$$x_{s+1,j}^0 = \mathrm{proj}_\Theta(x_{s,j}^0 - J(o_s)\frac{o_s - x_{s,j}^0}{J(o_s) - J(x_{s,j}^0)}),$$

where $\mathrm{proj}_\Theta : \mathbb{R}^N \to \Theta$ is the projection function for controlling that the new individuals fit into the search space Θ, defined as $\mathrm{proj}_\Theta(x)(k) = \min(\max(x(k), l_k), u_k)$, with $k = 1, \ldots, N$.

Step 4. Output: After $s_{\max}$ iterations, the GMA returns the following output:

$$GMAO(s_{\max}, N_{\mathrm{p}}, N_{\mathrm{g}}, p_{\mathrm{m}}, p_{\mathrm{c}}, \lambda, \hat{g}) = \mathrm{argmin}\{J(o_s)| \ s = 1, \ldots, s_{\max}\}.$$

This algorithm tries to improve, individual by individual, the initial population of the GA. More precisely, for each individual in the initial population:

- If there is a significant evolution of the cost function between this individual and o_s, the secant method generates a new individual close to o_s that performs a refined search near the current solution.
- Otherwise, the secant method creates a new individual far from o_s, to expand the exploration of the admissible space.

Moreover, when the GMA ends, its solution is improved by performing 10 iterations of the Steepest Descent (SD) algorithm, in which the descent step size ρ is determined using 10 iterations of a dichotomy method starting from $\rho_0 = 1$. This last layer of SD is carried out in order to enhance the accuracy of the final solution. This algorithm has been already tested for solving different computationally expensive industrial optimization problems (see, e.g., [24, 39, 33, 32]). Furthermore, it has been compared with other well-known metaheuristic method and it exhibits better performance for a set of Benchmark problems (see [36]). A Matlab version of the GMA presented in this paper has been implemented in the free optimization package "Global Optimization Platform" (GOP), which can be downloaded at http://www.mat.ucm.es/momat/software.html.

4. Numerical experiments

In this section, we first introduce the numerical solver used for computing the solutions of system (2.1)-(2.4). Then, in Section 4.2 we describe the considered numerical experiments based on the optimization problems (3.5), (3.6) and (3.9). Section 4.3 presents the optimization results, which are analyzed and compared in Section 4.4.

4.1. **Numerical implementation of the model.** The cylindrical version of system (2.1)-(2.4) was solved using the software COMSOL Multiphysics 5.0 (http://www.comsol.com), based on the Finite Element method (see [51]), with Lagrange P2-P1 elements to stabilize the pressure and to satisfy the Ladyzhenskaya, Babouska, and Brezzi stability condition. The 2nd-order Lagrange elements model the velocity and concentration components, while linear elements represent the pressure. At a first stage, we solve the stationary Navier-Stokes equations (2.4) using Galerkin least square streamline and crosswind diffusion methods so as to prevent numerical oscillations. At a second stage, the velocity field (solution of (2.4)) is introduced as an input value in the transient advection-diffusion-reaction system (2.1), which is then solved by considering an upwind scheme. We use a direct damped Newton method to solve the corresponding linear systems. A complete description of those techniques can be found in [22]. The numerical experiments

were carried out in a 2.8Ghz Intel i7-930 64bits computer with 12Gb of RAM. We used a triangular mesh with around 3000 elements, which produced significantly accurate results with respect to finer meshes that turned out to be computationally unreachable. We assumed that the solution of system (2.1) at finite time $\hat{T} = 10^7$ (s) could be considered as a reasonable approximation the steady state $(\hat{S}, \hat{B})$ of system (2.1). Model variables (3.2) and (3.3) were estimated using the functions *Domain Integration* and *Boundary Integration* of COMSOL (based on a trapezoidal approximation of the integral), respectively. Thus, the value of the cost function (3.4) was an output of the COMSOL model. After performing several numerical tests (as described in Section 3.1,) we have chosen $\beta = 10^9$ to be the value of the penalty parameter in the cost function as it has given good results for the considered numerical experiments. In this work, the GMA has been applied with $(s_{\max}, N_g, N_p, p_c, p_m, \lambda, \hat{g}) = (100, 10, 10, 0.4, 0.2, 1, 25)$ for solving numerically problems (3.5), (3.6) and (3.9). Those parameters had previously been successfully used for solving similar optimization problems in [9, 24, 39, 33]. Depending on the considered case (detailed below), each function evaluation in problems (3.5), (3.6) and (3.9) may take from 15 up to 60 minutes. With a restriction of 3 months of computational time to run the GMA, the number of function evaluations carried out to solve problems (3.5), (3.6) and (3.9) ranged between 2000 and 6000.

4.2. **Cases considered in this work.** Model parameters were set as follows (see [4, 63]): $D_S = 4.3 \cdot 10^{-12} (m^2/s)$, $D_B = 5 \cdot 10^{-10}$ (m^2/s), $S_{in} = 15$ (kg/m^3), $B_0 = 1$ (kg/m^3), $S_0 = 15$ (kg/m^3), $p_{atm} = 10^5$ (Pa), $\rho = 10^3$ (kg/m^3), $\eta = 10^{-3}$ $(kg/m\ s)$ and $u_{in} = 2.2 \cdot 10^{-4}$ (m/s). We consider four different reaction rate functions μ_1, μ_2, μ_3 and μ_4, which are described in Table 1 (see pages 132, 182 and 187 in [16]). In Figure 3, we plot those four growth rate functions. We can observe that they have the same order of magnitude but with different slopes.
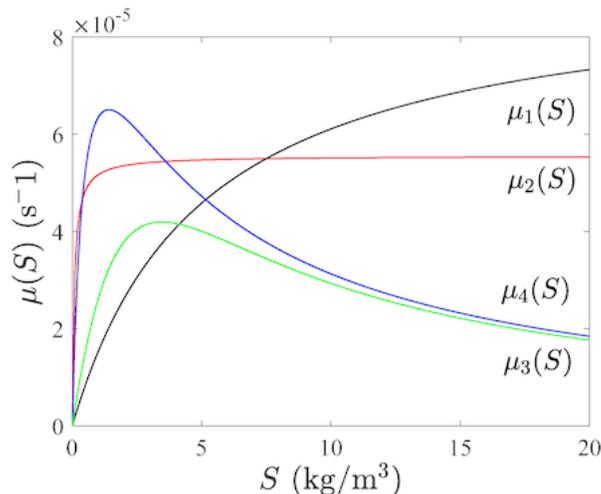

FIGURE 3. Functions $\mu_1(S)$, $\mu_2(S)$, $\mu_3(S)$ and $\mu_4(S)$ (s^{-1}), detailed in Table 1, with $S \in [0, 20]$ (kg/m^3).

TABLE 1. Considered growth rate functions

$\mu_1(\cdot)$	$\mu_2(\cdot)$
Monod function (2.2)	Monod function (2.2)
$\mu_{\max} = 9.17 \cdot 10^{-5} \text{ s}^{-1}$	$\mu_{\max} = 5.5 \cdot 10^{-5} \text{ s}^{-1}$
$K_{\mathrm{S}} = 5 \text{ kg/m}^3$	$K_{\mathrm{S}} = 0.075 \text{ kg/m}^3$
$\mu_3(\cdot)$	$\mu_4(\cdot)$
Haldane function (2.3)	Haldane function (2.3)
$\mu_{\max} = 1.39 \cdot 10^{-4} \text{ s}^{-1}$,	$\mu_{\max} = 1.11 \cdot 10^{-4} \text{ s}^{-1}$,
$K_{\mathrm{S}} = 4 \text{ kg/m}^3$,	$K_{\mathrm{S}} = 0.5 \text{ kg/m}^3$,
$K_{\mathrm{I}} = 3 \text{ kg/m}^3$	$K_{\mathrm{I}} = 4 \text{ kg/m}^3$

When solving problems (3.5) and (3.6), design parameters $H_{\min} = 2$ (m), $H_{\max} = 10$ (m) and $R_{\max} = 5$ (m) were taken to generate the admissible spaces $\tilde{\Phi}^1$ and $\tilde{\Phi}^2$. On the other hand, when solving problem (3.9), the admissible space $\tilde{\Phi}^3$ was generated with design parameters $H_{\min} = 2$ (m) $H_{\max} = 10$ (m) and $R_{1,\max} = R_{2,\max} = 3.5$ (m). In order to compute the values $E_{1,\min}$ and $E_{1,\max}$, we chose $R_{\max} = 5$ (m). In all cases we set $r = h = 0.5$ (m) and $S_{\lim} = 1$ (kg/m^3).

4.3. **Optimization results.** In this section, we present the optimization results obtained when solving problems (3.5), (3.6) and (3.9). Section 4.3.1 puts together the numerical results obtained when solving problems (3.5) and (3.6) because similar conclusions were obtained. We point out that in all the optimized reactors obtained in Sections 4.3.1 and 4.3.2, the optimal solutions $\tilde{\phi}^{i,\mathrm{opt}}$ are such that the second term in (3.4) is zero, and therefore, the value $J(\tilde{\phi}^{i,opt})$ corresponds to the reactor volume $\mathrm{Vol}(\tilde{\phi}^{i,\mathrm{opt}})$ ($i = 1, 2, 3$).

Remark 4.1. We observe from Tables 2-4 that the value $\hat{S}_{\mathrm{out}}(\tilde{\phi}^{i,\mathrm{opt}})$ ($i = 1, 2, 3$) is clearly smaller than the prescribed value $S_{\lim}$ in all the considered cases, which seems to indicate that smaller (and therefore better) domains could be obtained with this value closer to $S_{\lim}$. This inaccuracy may be due to the lack of numerical precision of the COMSOL model, which in turn is caused by the restriction on the computational time (see Section 4.1 for more details). This fact highlights the difficulties tackled during the numerical resolution of our optimization problem.

4.3.1. *Parametrizations 1 and 2.* Table 2 shows the optimal results when solving problem (3.5), while the optimized shapes are depicted in Figure 4. Similarly, Table 3 shows the optimal results when solving problem (3.6), while the optimized shapes are depicted in Figure 5.

From Figures 4 and 5 we observe that the optimal reactors have height larger than width. This outcome is in line with the results found in [56, 64], where the authors performed experimental studies to conclude that the most efficient reactor was a tubular one with its height much greater than its radius. Nevertheless, this strategy is not always applicable due to the practical restriction on the reactor height.

When comparing the results obtained with the reaction functions, we observe that the optimized reactors exhibit similar heights and the main difference lies in

TABLE 2. Value of the optimal parameters (H^{opt}(m) and R^{opt}(m)) in $\tilde{\phi}^{1,\mathrm{opt}}$, solution of (3.5) with functions $\mu_i, i = 1, \ldots, 4$; outflow substrate concentrations ($\hat{S}_{\mathrm{out}}(\tilde{\phi}^{1,\mathrm{opt}})$) (kg/ m^3); and reactor volumes (Vol($\tilde{\phi}^{1,\mathrm{opt}}$) m^3).

μ	H^{opt}	R^{opt}	$\hat{S}_{\mathrm{out}}(\tilde{\phi}^{1,\mathrm{opt}})$	Vol($\tilde{\phi}^{1,\mathrm{opt}}$)
μ_1	10	0.61	0.9528	11.3063
μ_2	9.82	0.66	0.9773	12.8553
μ_3	9.92	1.98	0.9718	110.6468
μ_4	9.9	1.6	0.9024	72.3634

TABLE 3. Value of the optimal parameters (H^{opt}(m) and R^{opt} (m)) in $\tilde{\phi}^{2,\mathrm{opt}}$, solution of (3.6) with functions $\mu_i, i = 1, \ldots, 4$; outflow substrate concentrations ($\hat{S}_{\mathrm{out}}(\tilde{\phi}^{2,\mathrm{opt}})$) (kg/ m^3); and reactor volumes (Vol($\tilde{\phi}^{2,\mathrm{opt}}$) (m^3).

μ	H^{opt}	R^{opt}	$\hat{S}_{\mathrm{out}}(\tilde{\phi}^{2,\mathrm{opt}})$	Vol($\tilde{\phi}^{2,\mathrm{opt}}$)
μ_1	9.28	0.728	0.9893	12.8479
μ_2	9.91	0.73	0.9558	13.8268
μ_3	9.98	1.96	0.9538	80.2715
μ_4	10	1.36	0.9216	40.6650

the reactor radius. For instance, the value of Vol($\tilde{\phi}^{1,\mathrm{opt}}$) (similarly, the value of Vol($\tilde{\phi}^{2,\mathrm{opt}}$)) is higher with μ_3 than with μ_1. This difference seems to be due to the fact that function μ_3 is qualitatively smaller than function μ_1 (see Figure 3) and thus, the optimal volume must be bigger to ensure that the prescribed value S_{lim} is reached. The influence of the reactor width on the bioreactor dynamics is explained in Remarks 4.2 and 4.3 later on.

4.3.2. *Parametrization 3.* Table 4 shows the optimal results, while the optimized shapes are depicted in Figure 6.

From Figure 6 we observe that, as stated in Section 4.3.1, the optimal reactors have height larger than width. Moreover, the exterior wall of the optimized reactors is concave, with a radius expansion observed at least in some limited part of the reactor (as said previously, the influence of the reactor radius in the bioreactor dynamics will be explained in Remarks 4.2 and 4.3 below). When comparing reaction functions, Figures 6-(a) and 6-(c) seem to show that, for instance, the radius expansion of the domain $\Omega(\tilde{\phi}^{3,\mathrm{opt}})$ is wider for growth rate function μ_3 than for μ_1, as observed in Section 4.3.1. On the other hand, the main difference between considering Monod (μ_1 and μ_2) or Haldane (μ_3 and μ_4) reaction functions is observed in the concavity at the upper part of the exterior wall (see Remark 4.2 for a physical interpretation).

4.4. **Comparison between the optimized reactors.** Here, we compare the solutions obtained when solving the optimization problems (3.5), (3.6) and (3.9).
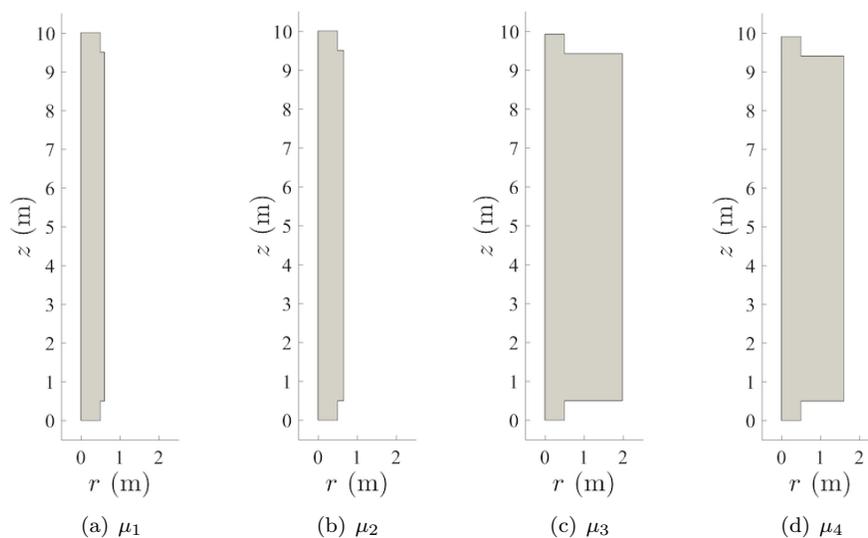
FIGURE 4. Shape of the optimized reactors, $\Omega(\tilde{\phi}^{1,\mathrm{opt}})$, where $\tilde{\phi}^{1,\mathrm{opt}}$ is the solution of problem (3.5).
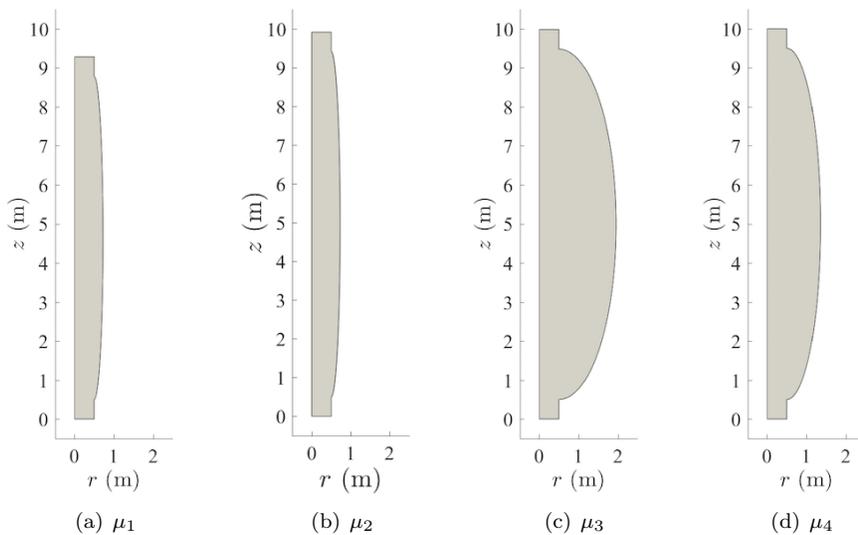

FIGURE 5. Shape of the optimized reactors, $\Omega(\tilde{\phi}^{2,\mathrm{opt}})$, where $\tilde{\phi}^{2,\mathrm{opt}}$ is the solution of problem (3.6).

Figures 4, 5 and 6 seem to show that the optimized reactors have height larger than width (indeed, $H_{\max}$ set to 10 (m) limits the optimal shape height and the optimal heights in all the considered cases approach this limit) and generally, the

TABLE 4. Value of the optimal parameters $(H^{\mathrm{opt}}(\mathrm{m}), R_1^{\mathrm{opt}}(\mathrm{m}), R_2^{\mathrm{opt}}(\mathrm{m}), \alpha_1^{\mathrm{opt}}$ and $\alpha_2^{\mathrm{opt}})$ in $\tilde{\phi}^{3,\mathrm{opt}}$, solution of (3.9) with functions $\mu_i, i = 1, \ldots, 4$; exterior control point coordinates (E_1 (m) and E_2 (m)), associated with $\tilde{\phi}^{3,\mathrm{opt}}$ and computed using equation (3.8) and Lemma 3.2; outflow substrate concentrations $(\hat{\mathrm{S}}_{\mathrm{out}}(\tilde{\phi}^{3,\mathrm{opt}})(\mathrm{kg/m}^3))$; and reactor volumes $(\mathrm{Vol}(\tilde{\phi}^{3,\mathrm{opt}})(\mathrm{m}^3))$.

μ	H^{opt}	R_1^{opt}	R_2^{opt}	α_1^{opt}	α_2^{opt}
μ_1	9.6359	0.5931	0.9214	$1.6358 \cdot 10^{-5}$	0.0059
μ_2	9.0814	0.5730	1.1024	0.0064	0.0922
μ_3	9.8879	2.0432	1.2402	0.0093	0.9940
μ_4	9.6401	1.0410	2.0805	$1.9301 \cdot 10^{-4}$	0.0273

μ	E_1	E_2	$\hat{\mathrm{S}}_{\mathrm{out}}(\tilde{\phi}^{3,\mathrm{opt}})$	$\mathrm{Vol}(\tilde{\phi}^{3,\mathrm{opt}})$
μ_1	0.3022	0.5512	0.9540	10.0790
μ_2	0.4111	1.2451	0.8923	12.0855
μ_3	-0.3928	8.8376	0.9545	27.1679
μ_4	-0.421	0.736	0.9962	22.3042

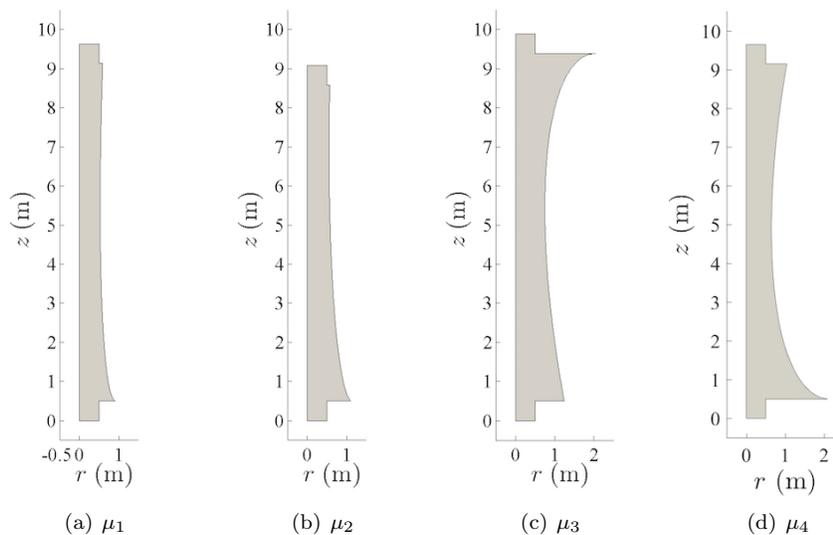(a) μ_1 (b) μ_2 (c) μ_3 (d) μ_4

FIGURE 6. Shape of the optimized reactors, $\Omega(\tilde{\phi}^{3,\mathrm{opt}})$, where $\tilde{\phi}^{3,\mathrm{opt}}$ is the solution of problem (3.9).

optimal widths approach its lower bound (the minimum reactor radius allowed was $r = 0.5$ (m)). However, in some of the considered cases (see Figures 4-(c), 4-(d), 5-(c), 5-(d), 6-(c) and 6-(d)), a radius expansion (at least in some limited part of

the reactor) is observed. We interpret that increasing the reactor width favors the reaction due to two main reasons:
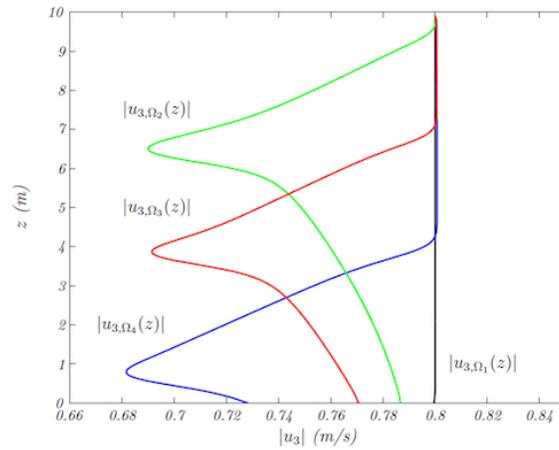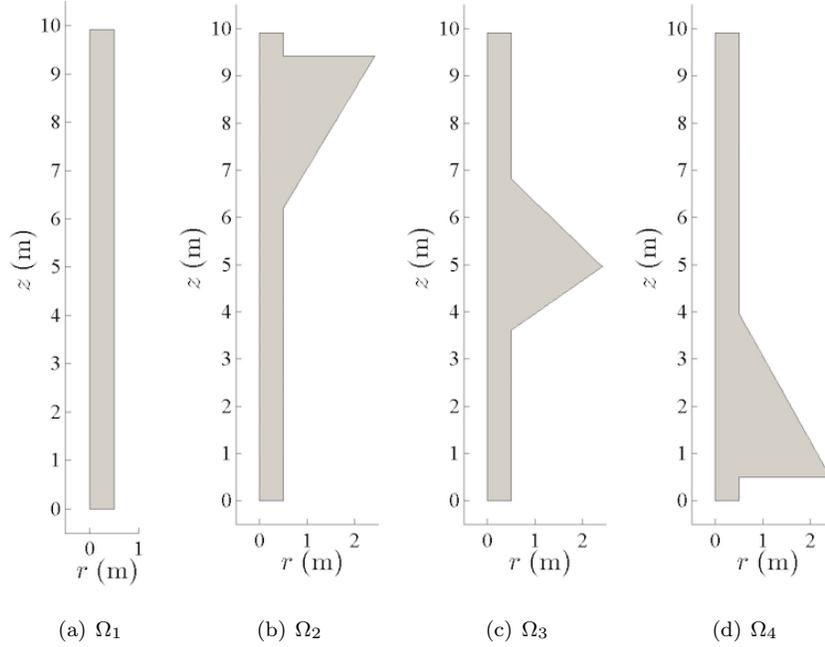
(1) It helps that the vertical flow velocity decreases (in absolute value), and so the time that the biomass and the substrate remain in contact for reacting increases (see Remark 4.2 for a more detailed analysis of the relation between the reactor width and the vertical flow).

(2) It originates an area of biomass storage. For example, due to the apparition of Dean vortices in this area (see, e.g., [13]) the biomass located near the device exterior wall remains more time inside the bioreactor (compared to the biomass located at the reactor center), and so the amount of reaction between biomass and substrate increases (see Remark 4.3 for an specific explanation about the distribution of substances in the reactor).

Remark 4.2. To understand the influence of the bioreactor width on the vertical flow velocity, we used four different domains, denoted by Ω_i, $i = 1, \ldots, 4$. The first reactor is cylindrical (depicted in Figure 7-(a)) and the other three present a radius extension on the top, center and bottom parts of the domain, (depicted in Figures 7-(b) to 7-(d), respectively). We solved system (2.4) with domains Ω_i, $i = 1, \ldots, 4$ and denoted u_{3,Ω_i} (m/s) the vertical flow velocity (third component of the velocity vector) obtained when solving system (2.4) in the domain Ω_i, evaluated at $r = 0$ (i.e., symmetry streamline). Figure 7-(e) represents $|u_{3,\Omega_i}|$, $i \in \{1, \ldots, 4\}$, which can be seen as functions of z. We observe that, in regions where the reactor radius increases, the absolute value of the vertical velocity decreases. This physical interpretation may explain, for instance, the optimal domains $\Omega(\tilde{\phi}^{3,\mathrm{opt}})$ obtained with reactions μ_3 and μ_4 (see Figures 6-(c) and 6-(d)), since the Haldane function shows inhibition for large values of substrate (see Figure 3) and the maximum value of substrate appears at the reactor inlet.

Remark 4.3. Figures 8-(a) and 8-(b) represent the distributions of substrate and biomass at steady state, respectively, computed with the optimal reactor $\Omega(\tilde{\phi}^{3,\mathrm{opt}})$, obtained for the growth rate function μ_3. One observes that the substrate is mainly agglomerated in the area originated by the inlet streamlines (see Figure 8-(d)). On the other hand, the biomass becomes withdrawn from this central area and is mainly concentrated around the reactor wall (where Dean vortices appear [13], see Figure 8-(d)). Thus, a reaction front is created between the central area and the outer part of the reactor (as shown in Figure 8-(c)) favoring the reaction between the two species. Although the optimization problems (3.5), (3.6) and (3.9) have been solved for a singular pair of diffusion coefficients (D_S, D_B), numerical experiments seem to show that the analysis of the distribution of substances in the reactor, performed above, is suitable in the range of typical diffusion coefficients D_S (from 10^{-10} to 10^{-7} (m^2/s) [46, 62, 65]) and D_B (from 10^{-13} to 10^{-7} (m^2/s) [25, 55, 60]).

Now, it is of interest to compare the optimized reactors obtained when solving the optimization problems (3.5), (3.6) and (3.9). In this direction, we denote by $d_r(\tilde{\phi}^i, \tilde{\phi}^j)$ ($i \neq j$) the relative difference between the optimal reactor volumes $\mathrm{Vol}(\tilde{\phi}^{i,\mathrm{opt}})$ and $\mathrm{Vol}(\tilde{\phi}^{j,\mathrm{opt}})$, defined as

$$d_r(\tilde{\phi}^i, \tilde{\phi}^j) = 100 \times \frac{\mathrm{Vol}(\tilde{\phi}^{j,\mathrm{opt}}) - \mathrm{Vol}(\tilde{\phi}^{i,\mathrm{opt}})}{\mathrm{Vol}(\tilde{\phi}^{i,\mathrm{opt}})}. \tag{4.1}$$

(a) Ω_1 (b) Ω_2 (c) Ω_3 (d) Ω_4

(e) Vertical velocity profile along the symmetry streamline
obtained for reactor domains Ω_i, $i = 1, \ldots, 4$.

FIGURE 7. Influence of the reactor width into the vertical flow velocity.

Table 5 shows the comparison, in terms of reactor volume, between the optimized reactors obtained when creating the domain with the three proposed parametrizations. Additionally, values $d_r(\tilde{\phi}^1, \tilde{\phi}^2)$ (resp. $d_r(\tilde{\phi}^1, \tilde{\phi}^3)$) are included in Table 5 in order to outline how much can be gained by using non-tubular reactors. One

(a) $\hat{S}(r,z)$ (kg/m³)   (b) $\hat{B}(r,z)$ (kg/m³)   (c) $\mu(\hat{S})\hat{B}$ (kg/m³ h)   (d) Streamlines
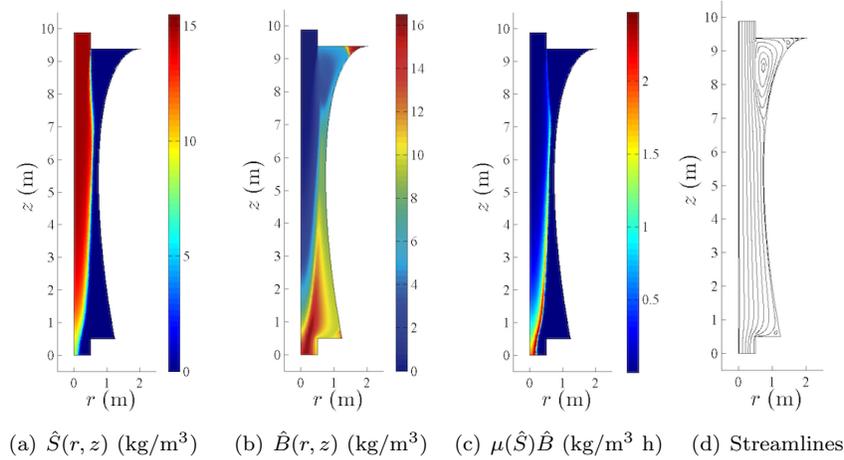
FIGURE 8. (a) substrate concentration (at steady state). (b) biomass concentration (at steady state). (c) reaction (at steady state) (d) streamlines. (a)-(d) associated with the optimal reactor $\Omega(\phi^{3,\mathrm{opt}})$ obtained for the growth rate function μ_3.

observes that for Monod growth rate functions (μ_1 and μ_2), the relative difference $d_r(\tilde{\phi}^1, \tilde{\phi}^j)$ ($j = 2, 3$) is between -10% and 13%, so one can conclude that the variation (in terms or reactor volume) between tubular and non-tubular reactors is relatively low. On the other hand, for Haldane growth rate functions (μ_3 and μ_4), one observes that by using non-tubular reactors, one can gain from 27% up to 75% in terms of reactor volume. Additionally, one may notice that the optimized reactor volumes differ substantially depending on the considered reaction function. Similar results have been obtained in other works focusing on the analysis of continuous bioreactors modeled through ordinary differential equations (see, e.g. [17, 26, 28, 29, 41])).

5. Conclusions

We have explored the shape design of a continuous biological reactor. The main objective was to reduce the reactor volume, ensuring that a prescribed output concentration value was reached at stationary state. As a matter of generalization, we have not imposed a particular type of biological dynamics in the reactor but proposed a general methodology to be applied and adapted depending on the considered case. We have used a mathematical model that couples hydrodynamics (described with the incompressible Navier–Stokes equations in three dimensions) with biological phenomena (described with an Advection-Diffusion-Reaction system). Using the Finite Element Method, we have numerically computed the output substrate concentration at steady state and the volume of a reactor associated with a particular set of design parameters. Then, we have defined three discrete optimization problems related to three different parametrizations of the device geometry and solved them by using a Genetic Multi-layer Algorithm, a self-implemented global optimization method based on the search of a suitable initial population for

TABLE 5. Comparison, in terms of reactor volume (m^3), between optimized reactors obtained when solving problems (3.5) (Vol($\tilde{\phi}^{1,\mathrm{opt}}$)), (3.6) (Vol($\tilde{\phi}^{2,\mathrm{opt}}$)) and (3.9) (Vol($\tilde{\phi}^{3,\mathrm{opt}}$)); relative differences $d_r(\tilde{\phi}^1, \tilde{\phi}^j)$ (%) ($j = 2, 3$) computed using equation (4.1).

μ	Vol($\tilde{\phi}^{1,\mathrm{opt}}$) (m^3)	Vol($\tilde{\phi}^{2,\mathrm{opt}}$) (m^3)	$d_r(\tilde{\phi}^1, \tilde{\phi}^2)$ (%)
μ_1	11.3063	12.8479	+13.63
μ_2	12.8553	13.8268	+7.56
μ_3	110.6468	80.2715	−27.45
μ_4	72.3334	40.6650	−43.78

μ	Vol($\tilde{\phi}^{3,\mathrm{opt}}$) (m^3)	$d_r(\tilde{\phi}^1, \tilde{\phi}^3)$ (%)
μ_1	10.0790	−10.85
μ_2	12.0855	−5.98
μ_3	27.1679	−75.45
μ_4	22.3042	−69.17

a given genetic algorithm. The optimization problem is solved for monotonic and non-monotonic growth rate functions, in order to analyze the influence of the reaction into the optimal reactor configuration. One of the proposed parametrizations allows us to model tubular shapes (typically used in the industry sector), while the other two offer the possibility to obtain a wider range of reactor geometries. We have taken into account that the reaction between species may be modeled by either monotonic or non-monotonic growth functions, and we have analyzed the influence of this factor on the optimization results.

From a general point of view, the optimized reactors exhibit height much larger than width and their exterior wall is concavely curved, with a radius expansion observed at least in some limited part of the reactor. The magnitude of the radius extension appears to be related to the reaction function. The slower is the reaction the wider should be the device. The advantage of the radius extensions in the reactor performance could be attributed to two main factors:

- The width of the reactor helps to decrease the absolute value of the vertical flow velocity, and consequently, increases the time of potential reaction between substances.
- The reactor corners may act as a biomass storage. The biomass located near the reactor exterior wall is withdrawn slower from the device than the biomass located near the device center, favoring the reaction between species.

When comparing the optimized reactors obtained for both monotonic and non-monotonic growth rate functions, one observes that, if the reactor is modeled with non-monotonic kinetics (e.g., Haldane function), the radius expansion located at the top of the reactor is more pronounced. We interpret that this difference relays on the fact that for large values of substrate (i.e., at the inlet of the device) the Haldane reaction shows inhibition, and so the radius expansion should be bigger to decrease the absolute value of the vertical flow near the reactor inlet.

An interesting message is that when the degrees of freedom on the shape parametrization is large enough, concavely curved reactors are systematically the best ones, although convexly curved (generated with less degrees of freedom) could already be better than perfect tubular shapes. The volume of the optimized reactors using concavely curved geometries (instead of typical tubular geometries) allow us to reduce the reactor volume between 25% and 90% depending on the considered case. This study shows to practitioners how much could be gained compared to the best cylindrical shapes, and how this gain is related to the reaction rate function (monotonic versus non-monotonic). Of course, the economic cost relative to the production of non-conventional should be taken into consideration for the best choice of the reactor geometry. Including this new (or other) criteria into the design problem should be tackled by using multi-objective approaches instead of single-objective approaches (see [20]).

References

[1] J. F. Andrews; *A mathematical model for the continuous culture of microorganisms utilizing inhibitory substrates*, Biotechnol. Bioeng., **10** (1968), no. 6, 707–723.

[2] J. L. Ansoni, P. Seleghim; *Optimal industrial reactor design: development of a multiobjective optimization method based on a posteriori performance parameters calculated from CFD flow solutions*, Adv. Eng. Softw., **91** (2016), no. C, 23–35.

[3] J. Antony; *Aerodynamic design via control theory*, J. Sci. Comput., **3** (1988), no. 3, 233–260.

[4] J. M. Bello, B. Ivorra, A. M. Ramos, A. Rapaport, J. Harmand; *Bioreactor shape optimisation. modeling, simulation, and shape optimization of a simple bioreactor for water treatment*, Les STIC pour l'environnement 2011, Lavoisier, 2011, pp. 125–141.

[5] J. P. Bitog, I.-B. Lee, C.-G. Lee, K.-S. Kim, H.-S. Hwang, S.-W. Hong, I.-H. Seo, K.-S. Kwon, E. Mostafa; *Application of computational fluid dynamics for modeling and designing photobioreactors for microalgae production: A review*, Comput. Electron. Agr., **76** (2011), no. 2, 131–147.

[6] E. F. Campana, D. Peri, Y. Tahara, F. Stern; *Shape optimization in ship hydrodynamics using computational fluid dynamics*, Comput. Methods Appl. Mech. Eng., **196** (2006), no. 1–3, 634–651.

[7] A. P. Carvalho, L. A. Meireles, F.X. Malcata; *Microalgal reactors: A review of enclosed system designs and performances*, Biotechnol. Prog., **22** (2006), no. 6, 1490–1506.

[8] T. Coenen, W. V. Moortel, F. Logist, J. Luyten, J. F. M. van Impe, J. Degrève; *Modeling and geometry optimization of photochemical reactors: Single- and multi-lamp reactors for UV–H_2O_2 AOP systems*, Chem. Eng. Sci., **96** (2013), 174–189.

[9] M. Crespo; *Mathematical modeling and optimization of bioreactors and liquid crystals*, Ph.D. thesis, Universidad Complutense de Madrid, 2017.

[10] M. Crespo, B. Ivorra, A. M. Ramos; *Existence and uniqueness of solution of a continuous flow bioreactor model with two species*, RACSAM A: Mat., **110** (2016), no. 2, 357–377.

[11] M. Crespo, B. Ivorra, A. M. Ramos; *Asymptotic stability of a coupled advection-diffusion-reaction system arising in bioreactor processes*, Electr. J. Differ. Equ., **2017** (2017), no. 194, 1–26.

[12] M. Crespo, A. M. Ramos, B. Ivorra, A. Rapaport; *Modeling and optimization of activated sludge bioreactors for wastewater treatment taking into account spatial inhomogeneities*, J. Process Contr. ,**54** (2017), 118–128.

[13] W. R. Dean; *The stream-line motion of fluid in a curved pipe (2nd paper)*, Lond. Edinb. Dubl. Phil. Mag. Sci., **5** (1928), no. 30, 673–695.

[14] K. Deb; *Multi-objective optimization using evolutionary algorithms*, Wiley Interscience Series in Systems and Optimization, Wiley, 2001.

[15] J. I. Díaz; *Remarks on the preceding paper by Crespo, Ivorra and Ramos on the stability of bioreactor processes*, Electr. J. Differ. Equ., **2017** (2017), no. 195, 1–25.

[16] D. Dochain; *Automatic control of bioprocesses*, ISTE, Wiley, 2010.

[17] D. Dochain, P. Vanrolleghem; *Dynamical modelling and estimation in wastewater treatment processes*, IWA Publishing, 2001.

[18] M. El-Sayed, T. Sun, J. Berry; *Shape optimization with computational fluid dynamics*, Adv. Eng. Softw., **36** (2005), no. 9, 607–613.

[19] G. Farin; *Curves and surfaces for computer-aided geometric design: A practical guide*, Computer science and scientific computing, Elsevier Science, 2014.

[20] M. R. Ferrández, S. Puertas-Martín, J. L. Redondo, B. Ivorra, A. M. Ramos, P. M. Ortigosa; *High-performance computing for the optimization of high-pressure thermal treatments in food industry*, J. Supercomput., (2018).

[21] P. Gajardo, H. Ramírez, A. Rapaport; *Minimal time sequential batch reactors with bounded and impulse controls for one or more species*, SIAM J. Control Optim., **47** (2008), no. 6, 2827–2856.

[22] R. Glowinski; *Numerical methods for nonlinear variational problems*, Scientific Computation, Springer Berlin Heidelberg, 2013.

[23] D. E. Goldberg; *Genetic algorithms in search, optimization, and machine learning*, Artificial Intelligence, Addison-Wesley, 1989.

[24] S. Gomez, B. Ivorra, A. M. Ramos; *Optimization of a pumping ship trajectory to clean oil contamination in the open sea.*, Math. Comput. Model, **54** (2011), no. 1, 477–489.

[25] S. E. Harding, P. Johnson; *The brownian diffusion of dormant and germinating spores of bacillus megaterium*, J. Appl. Bacteriol., **60** (1986), no. 3, 227–232.

[26] J. Harmand, D. Dochain; *The optimal design of two interconnected (bio)chemical reactors revisited*, Comput. Chem. Eng., **30** (2005), no. 1, 70–82.

[27] J. Harmand, C. Lobry, A. Rapaport, T. Sari; *The chemostat: Mathematical theory of microorganism cultures*, Wiley, 2017.

[28] J. Harmand, A. Rapaport, A. Trofino; *Optimal design of interconnected bioreactors: New results*, AIChE J., **49** (2003), no. 6, 1433–1450.

[29] G. A. Hill, C. W. Robinson; *Minimum tank volumes for CFST bioreactors in series*, Can. J. Chem. Eng., **67** (1989), no. 5, 818–824.

[30] D. Isebe, P. Azerad, F. Bouchette, B. Ivorra, B. Mohammadi; *Shape optimization of geotextile tubes for sandy beach protection*, Int. J. Numer. Meth. Eng., **74** (2008), no. 8, 1262–1277.

[31] B. Ivorra; *Application of the laminar navier–stokes equations for solving 2d and 3d pathfinding problems with static and dynamic spatial constraints: Implementation and validation in comsol multiphysics*, J. Sci. Comput., **74** (2018), no. 2, 1163–1187.

[32] B. Ivorra, M. R. Ferrández, M. Crespo, J. L. Redondo, P. M. Ortigosa, J. G. Santiago, A.M. Ramos; *Modelling and optimization applied to the design of fast hydrodynamic focusing microfluidic mixer for protein folding*, J. Math. Industry, **8** (2018), no. 4.

[33] B. Ivorra, J. López, A. M. Ramos, J.G. Santiago; *Design sensitivity and mixing uniformity of a micro-fluidic mixer*, Phys. Fluids (1994-present) **28** (2016), no. 1, 012005.

[34] B. Ivorra, B. Mohammadi, L. Dumas, O. Durand, P. Redont; *Semi-deterministic vs. genetic algorithms for global optimization of multichannel optical filters*, Int. J. Comput. Sci. Eng., **2** (2006), no. 3, 170–178.

[35] B. Ivorra, B. Mohammadi, A. M. Ramos; *Optimization strategies in credit portfolio management*, J. Global Optim., **42** (2009), no. 2, 415–427.

[36] B. Ivorra, B. Mohammadi, A. M. Ramos; *A multi-layer line search method to improve the initialization of optimization algorithms*, Eur. J. Oper. Res., **247** (2015), no. 3, 711–720.

[37] B. Ivorra, B. Mohammadi, J. G. Santiago, D. E. Hertzog; *Semi-deterministic and genetic algorithms for global optimization of microfluidic protein folding devices*, Int. J. Numer. Meth. Eng., **66** (2006), no. 2, 319–333.

[38] B. Ivorra, A. M. Ramos, B. Mohammadi; *Semideterministic global optimization method: Application to a control problem of the burgers equation*, J. Optimiz. Theory Appl., **135** (2007), no. 3, 549–561.

[39] B. Ivorra, J. L. Redondo, J. G. Santiago, P. M. Ortigosa, A. M. Ramos; *Two- and three-dimensional modeling and optimization applied to the design of a fast hydrodynamic focusing microfluidic mixer for protein folding*, Phys. Fluids (1994-present), **25** (2013), no. 3, 032001.

[40] R. J. LeVeque; *Finite difference methods for ordinary and partial differential equations: Steady-state and time-dependent problems*, Society for Industrial and Applied Mathematics, 2007.

[41] K. Ch. A. M. Luyben, J. Tramper; *Optimal design for continuous stirred tank reactors in series using Michaelis Menten kinetics*, Biotechnol. Bioeng., **24** (1982), no. 5, 1217–1220.

[42] R. A. E. Mäkinen, J. Periaux, J. Toivanen; *Multidisciplinary shape optimization in aerodynamics and electromagnetics using genetic algorithms*, Int. J. Numer. Methods Fluids, **30** (1999), no. 2, 149–159.

[43] F. Muyl, L. Dumas, V. Herbert; *Hybrid method for aerodynamic shape optimization in automotive industry*, Comput. Fluids, **33** (2004), no. 5-6, 849–858.

[44] V. Nejati, K. Matsuuchi; *Aerodynamics Design and Genetic Algorithms for Optimization of Airship Bodies*, JSME Int. J. Ser. B Fluids Therm. Eng., **46** (2003), no. 4, 610–617.

[45] J. Nocedal, S.J. Wright; *Numerical optimization, 2nd ed*, Springer New York, USA, 2006.

[46] R. Nogueira, L. F. Melo; *Competition between nitrospira spp. and nitrobacter spp. in nitrite-oxidizing bioreactors*, Biotechnol. Bioeng., **95** (2006), no. 1, 169–175.

[47] O. Pironneau; *Optimal shape design for elliptic systems*, Springer series in computational physics, Springer-Verlag, 1984.

[48] C. Poloni, A. Giurgevich, L. Onesti, V. Pediroda; *Hybridization of a multi-objective genetic algorithm, a neural network and a classical optimizer for a complex design problem in fluid dynamics*, Comput. Methods in Appl. Mech. Eng., **186** (2000), no. 2–4, 403–420.

[49] L. Pramparo, J. Pruvost, F. Stüber, J. Font, A. Fortuny, A. Fabregat, P. Legentilhomme, J. Legrand, C. Bengoa; *Mixing and hydrodynamics investigation using CFD in a square-sectioned torus reactor in batch and continuous regimes*, Chem. Eng. J., **137** (2008), no. 2, 386–395.

[50] H. Ramírez, A. Rojas, D. Jeison; *Productivity optimization of microalgae cultivation in a batch photobioreactor process*, Math. Methods Appl. Sci., (2017), 1–21.

[51] A. M. Ramos; *Introducción al análisis matemático del método de elementos finitos*, Editorial Complutense, 2012.

[52] J. L. Redondo, J. Fernández, I. García, P.M. Ortigosa; *Parallel algorithms for continuous competitive location problems*, Optim. Method Soft., **23** (2008), no. 5, 779–791.

[53] J. L. Redondo, J. Fernández, I. García, P.M. Ortigosa; *A robust and efficient global optimization algorithm for planar competitive location problems*, Ann. Oper. Res., **167** (2009), no. 1, 87–105.

[54] J. L. Redondo, J. Fernández, I. García, P.M. Ortigosa; *Solving the multiple competitive location and design problem on the plane*, Evol. Comput., **17** (2009), no. 1, 21–53.

[55] B. R. Reiter; *Assessment of laboratory methods for quantifying aqueous bacterial diffusion*, Master's thesis, University of Saskatchewan, 1999.

[56] A. Richmond, S. Boussiba, A. Vonshak, R. Kopel; *A new tubular reactor for mass production of microalgae outdoors*, J. Appl. Phycol., **5** (1993), no. 3, 327–332.

[57] J. C. Rodríguez, H. Ramírez, P. Gajardo, A. Rapaport; *Optimality of affine control system of several species in competition on a sequential batch reactor*, Int. J. Control, **87** (2014), no. 9, 1877–1885.

[58] R. R. Sharapov; *Genetic algorithms: Basic ideas, variants and analysis*, InTech, 2007.

[59] E. Sierra, F. G. Acién, J.M. Fernández, J. L. García, C. González, E. Molina; *Characterization of a flat plate photobioreactor for the production of microalgae*, Chem. Eng. J., **138** (2008), no. 1–3, 136–147.

[60] V. Singh; *Environmental hydrology*, Water Science and Technology Library, Springer Netherlands, 2013.

[61] H. Smith, P. Waltman; *The theory of the chemostat. in cambridge studies in mathematical biology*, vol. 13, Cambridge: Cambridge University Press, 1995.

[62] P. S. Stewart; *Diffusion in biofilms*, J. Bacteriol., **185** (2003), no. 5, 1485–1491.

[63] K. R. Symon; *Mechanics*, Addison-Wesley World student series, Addison-Wesley Publishing Company, 1971.

[64] M. R. Tredici, G. C. Zittelli; *Efficiency of sunlight utilization: Tubular versus flat photobioreactors*, Biotechnol. Bioeng., **57** (1998), no. 2, 187–197.

[65] R. T. Venterea, D. E. Rolston; *Mechanistic modeling of nitrite accumulation and nitrogen oxide gas emissions during nitrification*, J. Environ. Qual., **29** (2000), no. 6, 1741–1751.

[66] T. Weise; *Global optimization algorithms - theory and application*, Second ed., Self-Published, 2009.

[67] J.-Y. Xia, S.-J. Wang, S.-L. Zhang, J.-J. Zhong; *Computational investigation of fluid dynamics in a recently developed centrifugal impeller bioreactor*, Biochemical Engineering Journal, **38** (2008), no. 3, 406–413.

[68] W. Zuo; *An object-oriented graphics interface design and optimization software for cross-sectional shape of automobile body*, Adv. Eng. Softw., **64** (2013), 1–10.

Maria Crespo
Departamento de Matematica Aplicada a la Ingeniería Industrial, ETSII - Universidad Politécnica de Madrid, C José Gutiérrez Abascal 2, 28006 Madrid, Spain
Email address: maria.crespo@upm.es, Phone +34 913377370

Benjamin Ivorra
Instituto de Matemática Interdisciplinar & Departamento de Análisis Matemático y Matemática Aplicada, Universidad Complutense de Madrid, Plaza de Ciencias, 3, 28040 Madrid, Spain
Email address: ivorra@ucm.es

Angel Manuel Ramos
Instituto de Matemática Interdisciplinar & Departamento de Análisis Matemático y Matemática Aplicada, Universidad Complutense de Madrid, Plaza de Ciencias, 3, 28040 Madrid, Spain
Email address: angel@mat.ucm.es

Alain Rapaport
MISTEA, Université Montpellier, INRA, Montpellier SupAgro. 2 Place P.Viala, 34060 Montpellier, France
Email address: rapaport@supagro.inra.fr